INTERNATIONAL JOURNAL OF GEOMAGNETISM AND AERONOMY
VOL. 3, NO. 1, PAGES 5–18, JANUARY 2002

Effects of solar wind dynamic pressure and magnetosonic Mach number on the bow shock, and the possible occurrence of erosion: 18–19 October 1995

S. Mühlbachler,[1] C. J. Farrugia,[2] H. K. Biernat,[3] D. F. Vogl,[3] V. S. Semenov,[4] P. Aber,[5] J. M. Quinn,[2] N. V. Erkaev,[6] K. W. Ogilvie,[7] R. P. Lepping,[7] S. Kokubun,[8] and T. Mukai[9]

[1]Space Research Institute, Austrian Academy of Sciences, Graz, Austria
[2]Institute of the Study of Earth, Oceans, and Space, University of New Hampshire, Durham, New Hampshire, USA
[3]Space Research Institute, Austrian Academy of Sciences, Graz, Austria
[4]Institute of Physics, St. Petersburg State University, St. Petersburg, Russia
[5]Faculty of Arts and Sciences, Harvard University, Cambridge, Massachusets, USA
[6]Institute of Computational Modelling, Russian Academy of Sciences, Krasnojarsk, Russia
[7]NASA Goddard Space Flight Center, Greenbelt, Maryland, USA
[8]Solar–Terrestrial Environment Laboratory, Nagoya University, Nagoya, Japan
[9]Institute of Space and Astronautical Science, Kanagawa, Japan

Abstract. We study the position and motion of the bow shock during the passage of the 18–19 October 1995, interplanetary magnetic cloud. The Geotail spacecraft made 26 bow shock crossings while it was nominally crossing the dawnside magnetosheath on a west–east trajectory approaching the Sun–Earth line. Interplanetary parameters are measured by the Wind spacecraft. The effects of changes in solar wind dynamic pressure and magnetosonic Mach number, which fall into three groups depending on interplanetary conditions, are studied and their respective effects are separated. Observed bow shock positions are compared with the model bow shock standoff distances [after *Cairns and Lyon*, 1995] and show good agreement. Finally, we calculate the magnetopause standoff distance on the basis of pressure balance between solar wind dynamic pressure and the Earth magnetic field magnetic pressure and compare these results with a magnetopause standoff distance derived from the *Shue et al.* [1998] model. We find that the magnetopause standoff distance during the cloud passage is larger than the *Shue et al.* [1998] result. We attribute this to magnetosphere erosion and note that solar wind conditions on this day show all prerequisites necessary for erosion.

Magnetic Cloud Event, 18–19 October 1995

The magnetic cloud that passed Earth on 18–19 October 1995 (see Figure 1), caused the largest geomagnetic storm in the period between 1994 and 1997 ($Dst = -120$ nT). The cloud has been intensely studied by the scientific community [see, e.g., *Burlaga et al.*, 1998; *Farrugia et al.*, 1998; *Lepping et al.*, 1997]. It was observed by the Wind space-

Paper number GAI01354.
CCC: 1524–4423/2002/0301–0354$18.00

The online version of this paper was published 24 August 2001.
URL: http://ijga.agu.org/v03/gai01354/gai01354.htm
Print companion issued January 2002.

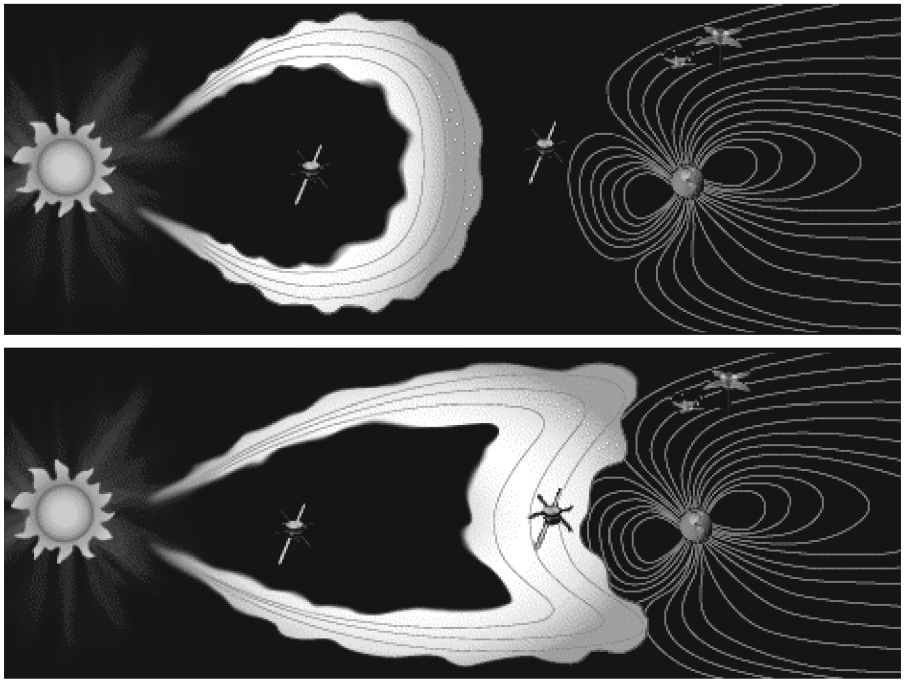

Figure 1. A sketchy introduction to the magnetic cloud of 18–19 October 1995.

craft upstream of Earth when the spacecraft was located at an average radial distance of ∼175 R_E.

Magnetic clouds are very useful for investigating the interaction between the solar wind and the magnetosphere because of their special properties, which allow them to couple energy and momentum to the magnetosphere, thus driving storms and substorms. Interplanetary magnetic clouds are characterized by (1) strong magnetic field strengths relative to ambient values, (2) low proton β and proton temperature, and (3) large and smooth rotation of magnetic field direction [*Burlaga et al.*, 1981; *Lepping et al.,* 1990].

Their passage at Earth typically lasts about 1–2 days, and their dimension at AU is ∼0.25 AU. Furthermore, magnetic clouds are often a dramatic source of long–lasting, strong, negative B_z of interplanetary magnetic field, which is an optimum condition for reconnection at the dayside magnetopause. Ahead of fast magnetic clouds, interplanetary shocks are often observed [*Burlaga*, 1995].

Normally, magnetic clouds have low Alfvén, $M_{\rm A}$, and magnetosonic, $M_{\rm ms}$, Mach numbers [*Farrugia et al.,* 1995]. Thus the Earth's bow shock may be expected to be displaced sunward with respect to its statistical position, as given e.g., by *Fairfield* [1971]. During the cloud event, the Geotail spacecraft crossed the magnetosheath on a dawn-to-dusk orbit. Its trajectory is shown in Figure 2, where we have superposed on the (YZ), (XZ), and (XY) projections (in GSE coordinates) of the 26 bow shock crossings, which are all located on dawnside ($Y < 0$) and indicated by crosses.

Wind Observations

The key parameter data we examine are as follows. Plasma data are from the SWE (Wind) and from the LEP instruments (Geotail). Magnetic field data are obtained from MFI and MGF instruments [e.g., *Kokubun et al.* 1992; *Lepping et al.* 1995; *Mukai et al.*, 1992; *Ogilvie et al.*, 1995].

Wind proton and magnetic field data are plotted in Figure 3. The panels show from top to bottom the density ($\rm cm^{-3}$), bulk speed (km $\rm s^{-1}$), temperature (K), the GSE X, Y, Z components of the interplanetary magnetic field (nT), and its strength (nT). The bottom two panels show the magnetosonic Mach number and the solar wind dynamic pressure (nPa).

The magnetic cloud arrived at Wind at approximately 1900 UT on 18 October 1995, preceded by an interplanetary shock at ∼1040 UT. The magnetic field turned abruptly and strongly southward when Wind entered the magnetic cloud, and it rotated gradually to a northward orientation during the next ∼24 hours. The magnetic field strength in the cloud was large (20–30 nT) and relatively constant. Note the relatively constant bulk speed in the cloud. The magnetosonic Mach number in the cloud is very low (between 2 and 4), which is ideal to check the position of the bow shock because this is precisely the range where in MHD theories the standoff distance starts to increase.

Solar wind dynamic pressure is high in the cloud's sheath

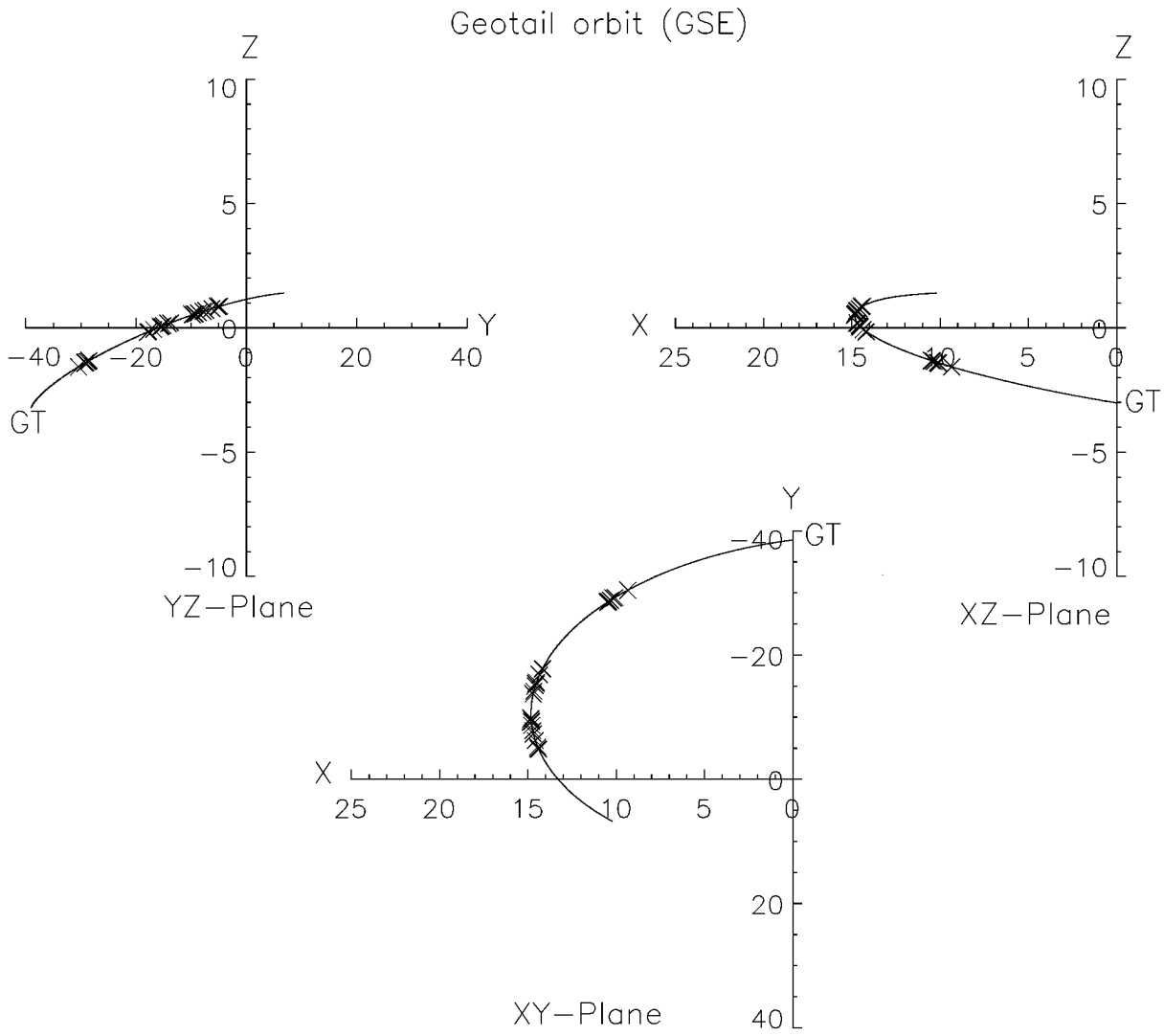

Figure 2. Geotail orbit from dawn to dusk in three planes and the shock crossings, which are indicated by crosses.

and very low inside the cloud with a gradual increase from ∼1 nPa up to ∼10 nPa. This increase is mainly due to the interaction with a faster trailing stream [*Farrugia et al.,* 1998].

Most of the time $p_{\rm dyn}$ is below the historical average of 2.2 nPa. The interplanetary parameters provide an ideal situation to examine the bow shock position as a function of low magnetosonic Mach number and under a wide range of dynamic pressure from $0.2 < p_{\rm dyn} < 10$ nPa in the cloud.

Geotail Observations

Figure 4 shows an overplot of Wind and Geotail data, where the Wind data have been shifted by the average delay time of ∼43 min. From top to bottom the figure shows the solar wind density ($\rm cm^{-3}$), the solar wind bulk speed ($\rm km\ s^{-1}$), the GSE X, Y, Z components of the interplanetary magnetic field (nT), and its strength (nT). Geotail is initially in the solar wind when the sheath of the cloud passes. When the cloud arrives, B_z measured by Geotail (GT) suddenly drops to a large negative value of about ∼ (−45) nT and the bow shock moves outward and GT is located in the magnetosheath. Each time GT is in the solar wind we can see good agreement at the two spacecrafts, and vice versa when the bow shock moves out and Geotail is in the Earth's magnetosheath. From the measurements made by Geotail we can identify five different periods of IMF and plasma behavior of the solar wind (Table 1), three periods with bow shock crossings, two without.

Shape and Location of the Bow Shock

In a statistical analysis, *Farris et al.* [1991] studied 351 independent bow shock crossings and 233 independent mag-

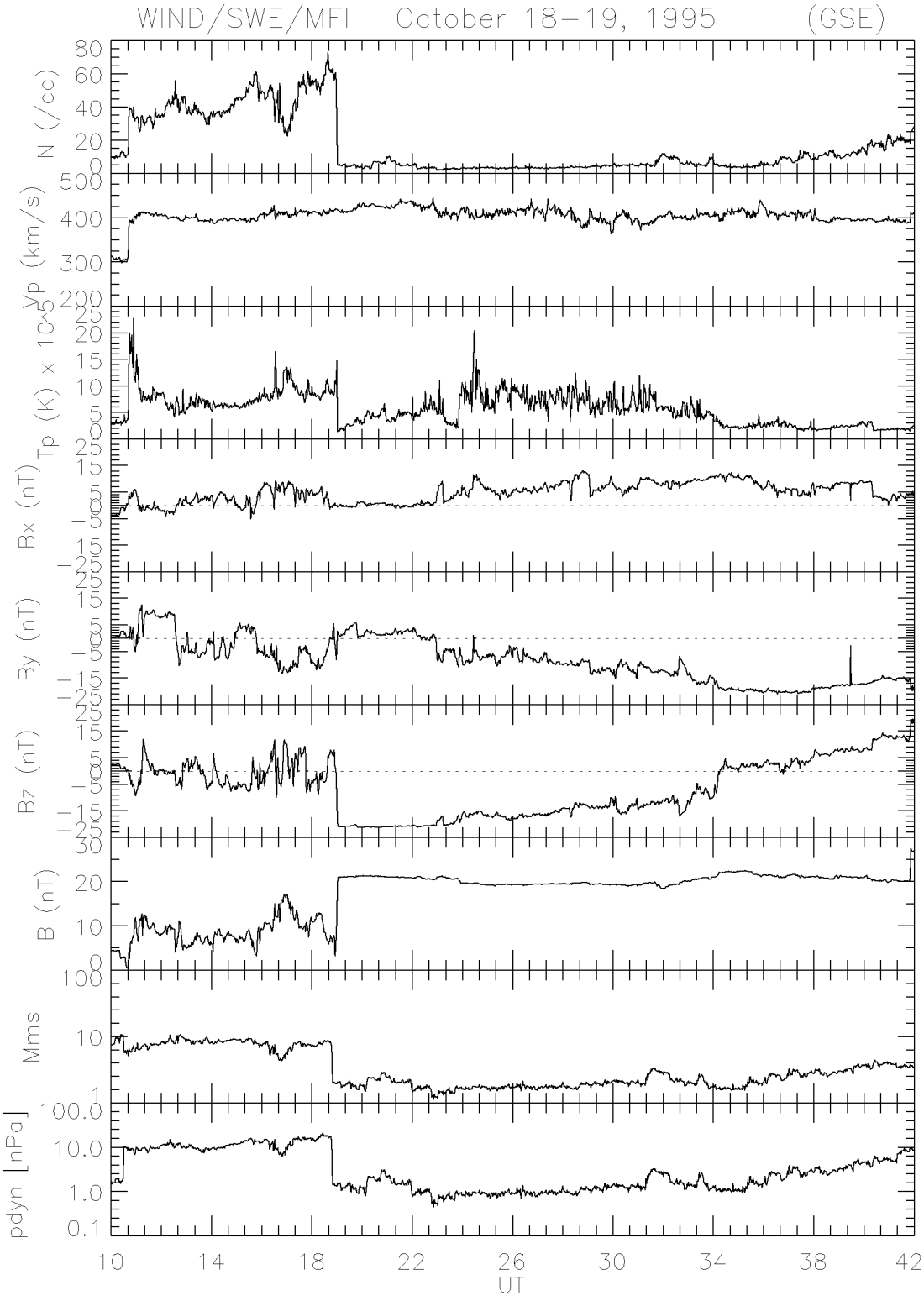

Figure 3. Data from Wind spacecraft from 18 October 1995, 1000 UT, to 19 October 1995, 1800 UT.

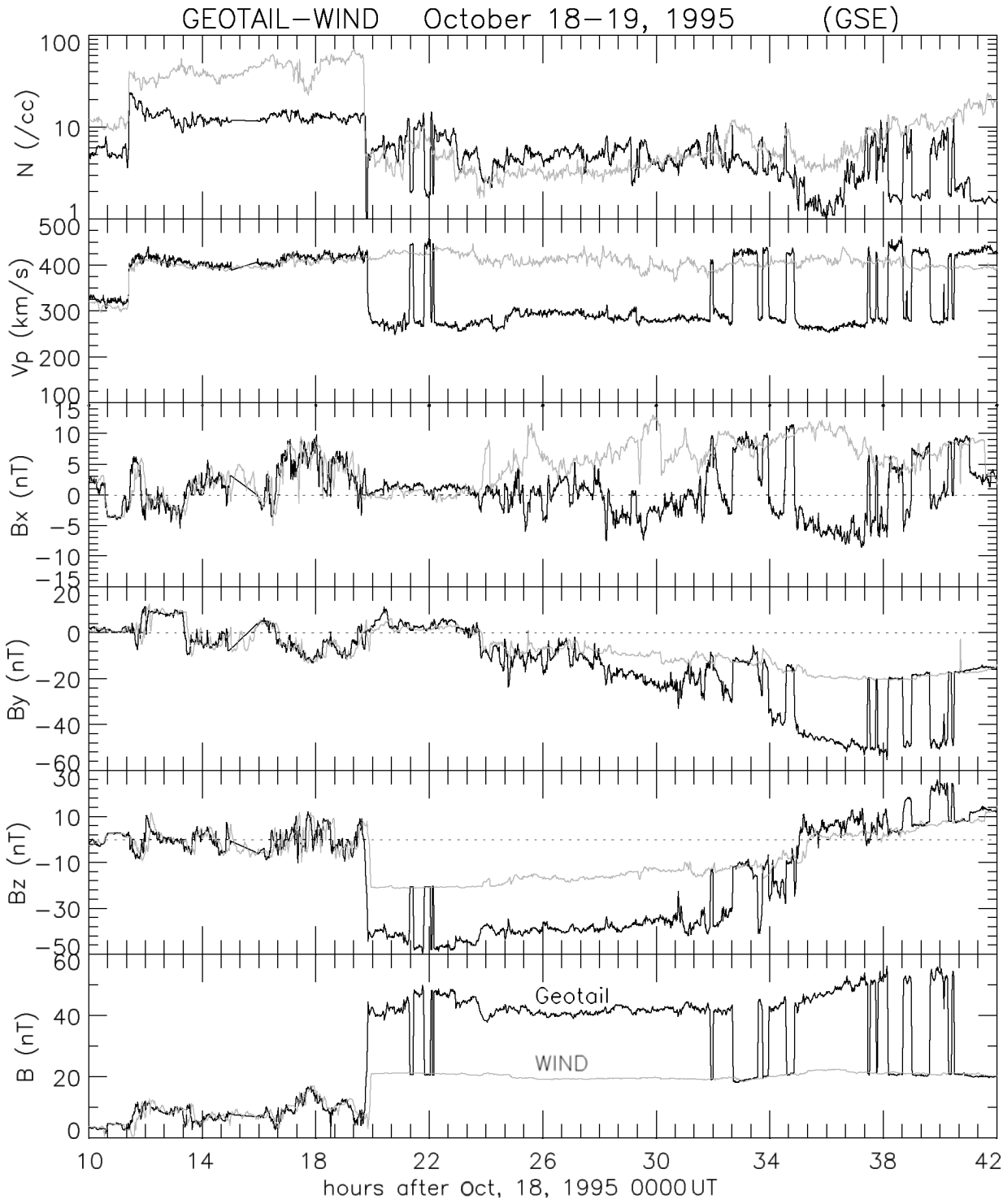

Figure 4. Data from Wind and Geotail spacecrafts from 18 October 1995, 1000 UT, to 19 October 1995, 1800 UT. Wind data are shifted by an average delay of ∼43 min.

netopause crossings made by the ISEE 1 spacecraft from 1977 to 1980 to determine the average positions and shapes of the bow shock and the magnetopause. They represented the bow shock as a paraboloid and obtained statistically $X = a_s - b_s(Y^2 + Z^2)$ and $a_s = 13.7 \pm 0.2\,R_E$ and $b_s = 0.0223 \pm 0.0003\,R_E^{-1}$ for the subsolar standoff distance and the shape parameters, respectively.

Specifically for low Alfvén Mach numbers, *Farrugia et al.*

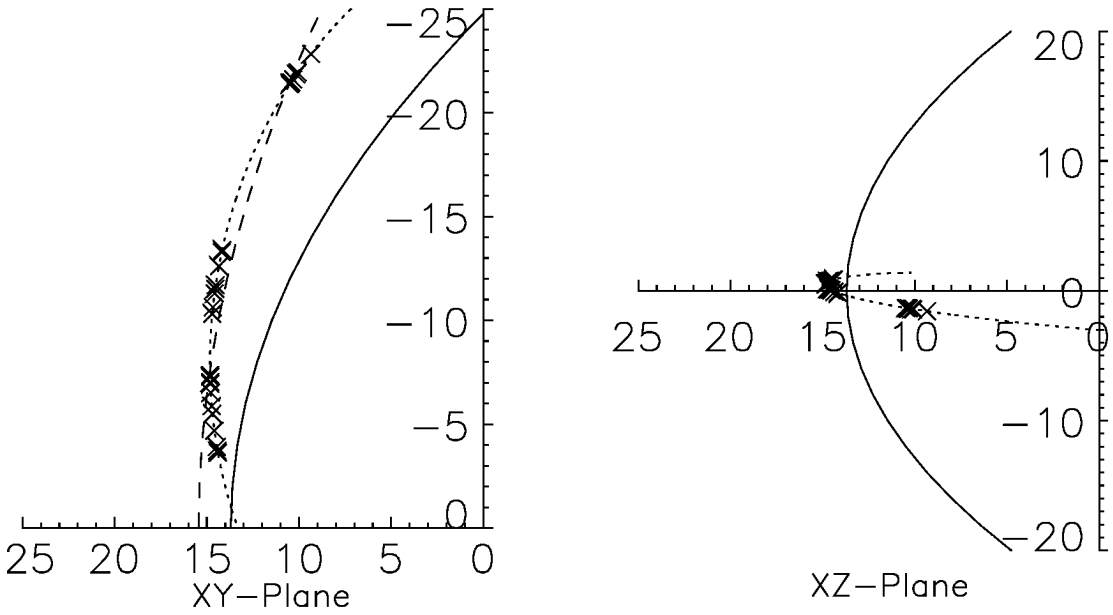

Figure 5. Geotail trajectory (dotted) and shock crossings (marked by crosses). The $1/M_A^2$ fitted bow shock (dashed) is compared with the *Farris et al.* [1991] bow shock (solid).

[1995] derived a quasi-linear connection between the thickness of the magnetosheath $D_{\rm ms}$ normalized to the subsolar radius of the magnetopause $a_{\rm mp}$ ($D_{\rm ms}(a_s - a_{\rm mp})/a_{\rm mp}$) and the inverse square of the Alfvén Mach number, $1/M_{\rm A}^2$, as it is in our study.

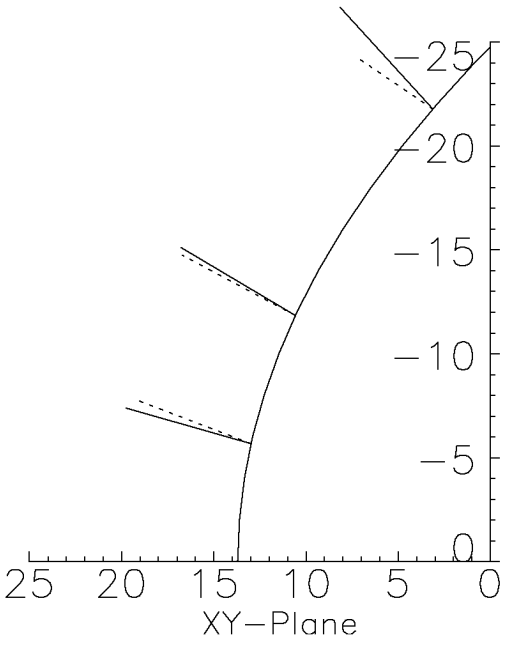

Figure 6. Farris et al. bow shock shape and the bow shock normals, on average, for each group of crossings: solid line, normal of the Farris shape; dotted line, normal from coplanarity [*Abraham-Shrauner and Yun,* 1976].

Therefore, ignoring the motion of the bow shock, we fit the crossings to the *Farris et al.* [1991] formula to a functional form which brings out the $1/M_{\rm A}^2$ dependence explicitly. Instead of two parameters, a_s and b_s, in the Farris formula, a four-parameter formula is employed:

$$X = \left(a_1 + \frac{a_2}{M_{\rm A}^2}\right) - \left(a_3 + \frac{a_4}{M_{\rm A}^2}\right)(Y^2 + Z^2) \qquad (1)$$

Least squares fitting yields $a_1 = 13.37$, $a_2 = 12.97$, $a_3 = 0.005$, and $a_4 = 0.036$.

Figure 5 shows the trajectory of Geotail (dotted) in the XY and XZ plane approaching the subsolar line from the dawnside. Crosses on this trajectory mark the 26 bow shock crossing as seen by Geotail. The solid curve represents the *Farris et al.* [1991] bow shock, whereas the dashed curve shows our fitted bow shock. With respect to the Farris et al. formula, our bow shock is, on average, displaced by 1.85 R_E sunward. If we consider the second period (Table 1) with its unusually low and rather constant values of $M_{\rm ms}$ and $p_{\rm dyn}$ and no bow shock crossings, we may conclude that the bow shock must have been sunward of the orbit of Geotail. Otherwise, crossings occur when either $p_{\rm dyn}$ and/or $M_{\rm ms}$ vary; see, for example, period 1 from 1900–2300 UT in Figure 3 in the bottom two panels.

Bow Shock Normals

We employ two different methods of calculating the bow shock normals: (1) from the shape of the Farris et al. bow shock and (2) from the coplanarity theorem [after *Abraham-Shrauner and Yun*, 1976].

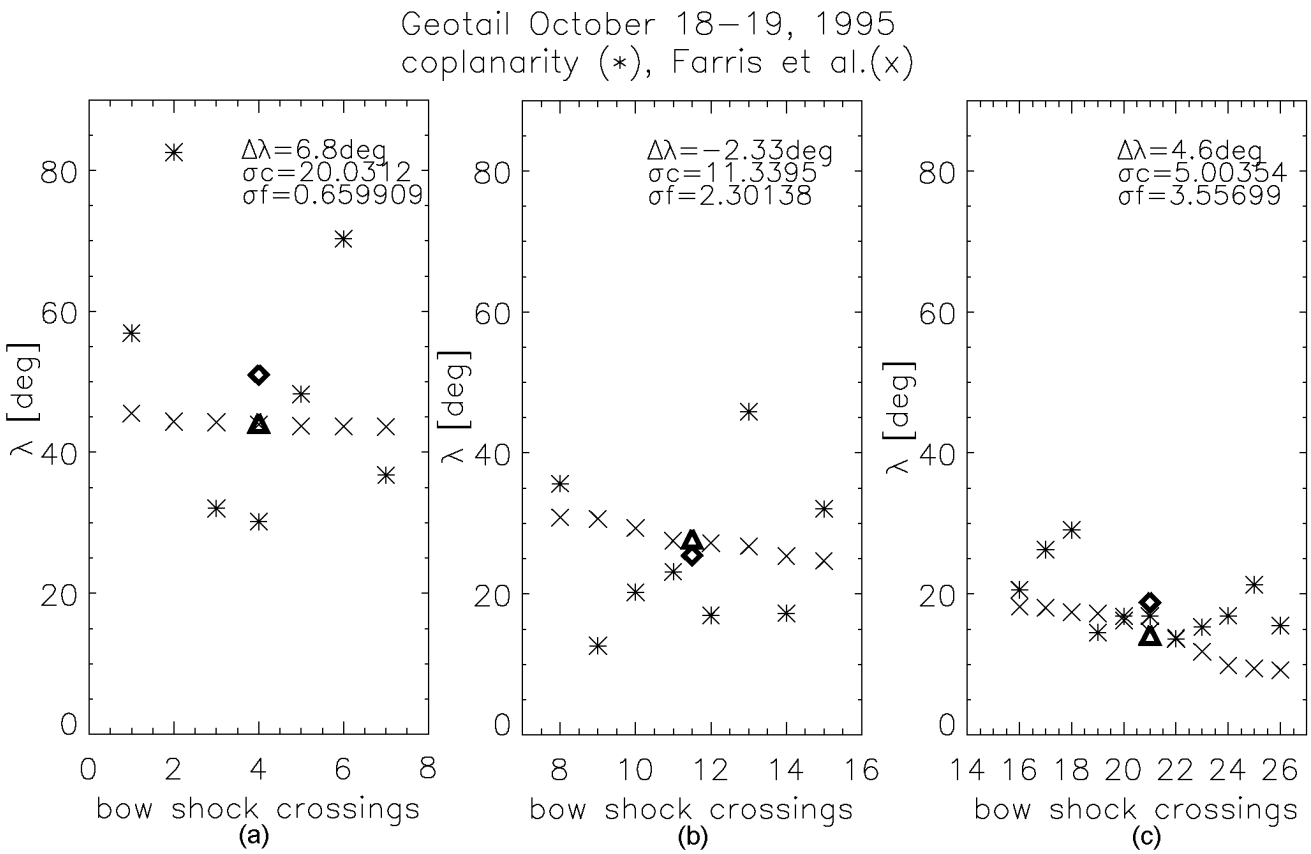

Figure 7. (a–c) Angles λ between the derived bow shock normals and the subsolar line for each group of crossings. Triangles and diamonds are the average angles for each group; σ_f and σ_c are the standard deviations for the two methods.

For method (1) we know the position vector $\mathbf{r}$ of the boundary

$$\mathbf{r} = \begin{pmatrix} 13.7 - 0.0223(Y^2 + Z^2) \\ Y \\ Z \end{pmatrix} \tag{2}$$

Thus the shock normal vector at any point at the curve can be derived from vector analysis

$$\mathbf{n}_{BS} = \frac{\partial \mathbf{r}}{\partial Y} \times \frac{\partial \mathbf{r}}{\partial Z} \begin{pmatrix} 1 \\ 0.0446\, Y \\ 0.0446\, Z \end{pmatrix} \tag{3}$$

For the shock normal derived from the coplanarity theorem we compute upstream and downstream values of the magnetic field and obtain

$$\mathbf{n}_{BS} = \frac{(\mathbf{B}_1 \times \mathbf{B}_2) \times (\mathbf{B}_1 - \mathbf{B}_2)}{|(\mathbf{B}_1 \times \mathbf{B}_2) \times (\mathbf{B}_1 - \mathbf{B}_2)|} \tag{4}$$

where subscripts 1 and 2 refer to upstream and downstream values of $\mathbf{B}$.

Figure 6 shows the Farris et al. bow shock shape and the normals, mentioned above, averaged for the three periods of shock crossings. The solid line normal refers to calculation 1 and the dotted line to calculation 2, respectively.

Table 1. Five Periods of Average $M_{\rm ms}$ and $p_{\rm dyn}$ and Different IMF Orientation and Number of Bow Shock Crossings

Geotail Time, UT	Number of Crossings	$\overline{M_{\rm ms}}$	$\overline{p_{\rm dyn}}$, nPa	B_y	B_z
1949–2209	7	2.09	1.61	slightly positive	strongly negative
2210–3153	–	1.77	1.01	slightly negative	negative
3154–3451	8	2.41	1.97	strongly negative	rotates to positive
3452–3725	–	1.99	1.66	strongly negative	slightly positive
3726–4029	11	3.11	3.48	strongly negative	positive

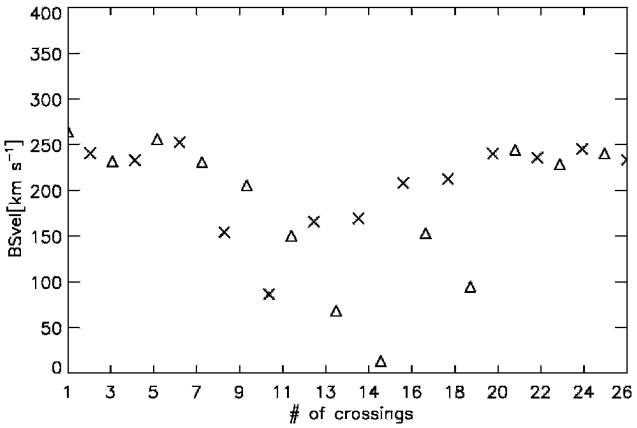

Figure 8. Bow shock velocities inbound crosses and outbound triangles.

In Figure 7 we plot for each interval the angle λ between the derived shock normals and the subsolar line, also for each method. The observed normal directions have large scatter, which however decreases in groups 2 and 3, i.e., as Geotail approaches the subsolar line. The large scatter of the coplanarity normals in group 1 (at the flanks of the bow shock) may be due to localized disturbances on the shock and hint to a more fluttery shock shape at the flanks. The last group, where the scatter is small still has $\Delta\lambda = 4.6°$. This may indicate that the actual bow shock shape departs from an axisymmetrical shape, what may be due to the large B_y component of the cloud field at this time.

The angles θ between the shock normals and the IMF B_n at each bow shock crossing are all $\theta > 45°$, and thus all shock crossings are perpendicular shocks.

Velocity of the Bow Shock

Now we use the coplanarity normals to derive the bow shock velocity after *Burgess* [1995]

$$v_{\rm shock} = \frac{\rho_2\,\mathbf{v}_2 - \rho_1\,\mathbf{v}_1}{\rho_2 - \rho_1}\,\mathbf{n}_{BS} \qquad (5)$$

The velocities of the bow shock at each crossing are plotted in Figure 8. Crosses and triangles mark whether the bow shock is moving outward or inward. The first and the last group of crossings all have a velocity of the order of $\sim$250 km s^{-1}, whereas the second group has a large scatter and lower velocities down to $\sim$20 km s^{-1}, what is probably due to the small density jumps across the bow shock during period 2 (see Geotail measurements in Figure 4).

Effects of Dynamic Pressure and Mach Numbers

The magnetosonic Mach number is very low at times of shock in and out motions, between 1.2 and 3. The trend for large sunward displacement for decreasing $M_{\rm ms}$ is evident here. It has been shown in previous studies [e.g., *Cairns and Grabbe*, 1994; *Cairns and Lyon*, 1995, 1996; *Cairns et al.,* 1995; *Fairfield*, 1971; *Farris et al.,* 1991; *Formisano et al.*, 1971; *Grabbe,* 1997; *Peredo et al.,* 1995] that at very low Alfvén and magnetosonic Mach numbers the subsolar distance could increase up to 30 or more R_E. Note, however, that we never observe a static bow shock but one moving either earthward or sunward.

We now discuss the dynamic pressure. For an increasing dynamic pressure, the magnetopause standoff distance moves inward, as does the bow shock. We assume here that this is the primary effect of dynamic pressure. We shall therefore not study changes of the shape of the magnetosphere (blunt to more pointed), which rapid and large dynamic pressure changes may be expected to occasion; that is, we shall consider in first approximation only changes in dynamic pressure, which are slow, i.e., which affect the whole magnetosphere. The crossings are obviously correlated with changes in dynamic pressure. When the dynamic pressure is low and < 1 nPa, there are no crossings at all; that is, the $M_{\rm ms}$ and the $p_{\rm dyn}$ effects on the bow shock position act in the same direction.

In Figure 9 we superpose dynamic pressure, magnetosonic Mach number, and the magnetic field at Geotail for the three sets of crossings. The figure shows that there is a clear extra response delay of about 10–20 min, for both inward and outward motion (see, e.g., rise of $p_{\rm dyn}$ at 2105 UT in the top panel and at 3225 UT in the middle panel). This is probably mainly due to the delay for changes in $M_{\rm ms}$ and $p_{\rm dyn}$ seen at Geotail to reach the bow shock and subsequently for the bow shock to cross the Geotail position. For outward motions it could be that $p_{\rm dyn}$ and $M_{\rm ms}$ change slowly, and the bow shock approached Geotail without crossing it, but it does later after a further impulsive drop in magnetosonic Mach number.

Much work has been done on the bow shock standoff distance as a function of interplanetary parameters [see e.g. *Grabbe and Cairns*, 1995, and references therein]. In recent years there is renewed interest on this issue for cases when the Alfvén Mach number is low [*Cairns and Grabbe*, 1994; *Cairns et al.*, 1995; *Russell and Petrinec*, 1996a, 1996b]. In their paper, *Grabbe and Cairns* [1995] present an analytical MHD formula for the density jump $\rho_2/\rho_1 = X$

$$\begin{aligned} X &= \frac{(\gamma-1)}{(\gamma+1)} + \frac{2}{(\gamma+1)}\left[\frac{1}{M_S^2} + \frac{\sin^2\theta}{(\gamma-1)M_{\rm A}^2}\right] \\ &+ \frac{2\sin^2\theta}{(\gamma-1)^2 M_{\rm A}^2}\left[\frac{\gamma\cos^2\theta}{(\gamma-1)M_{\rm A}^2}\right. \\ &+ \left.(\gamma-2)\left(\frac{1}{M_S^2} + \frac{1}{(\gamma-1)M_{\rm A}^2}\right)\right] \end{aligned}$$

Because of the perturbation technique used to derive this formula, it is valid only for values of $\theta \leq 60°$. In our case, where the average value of $\theta \sim 75°$, one has to take a sim-

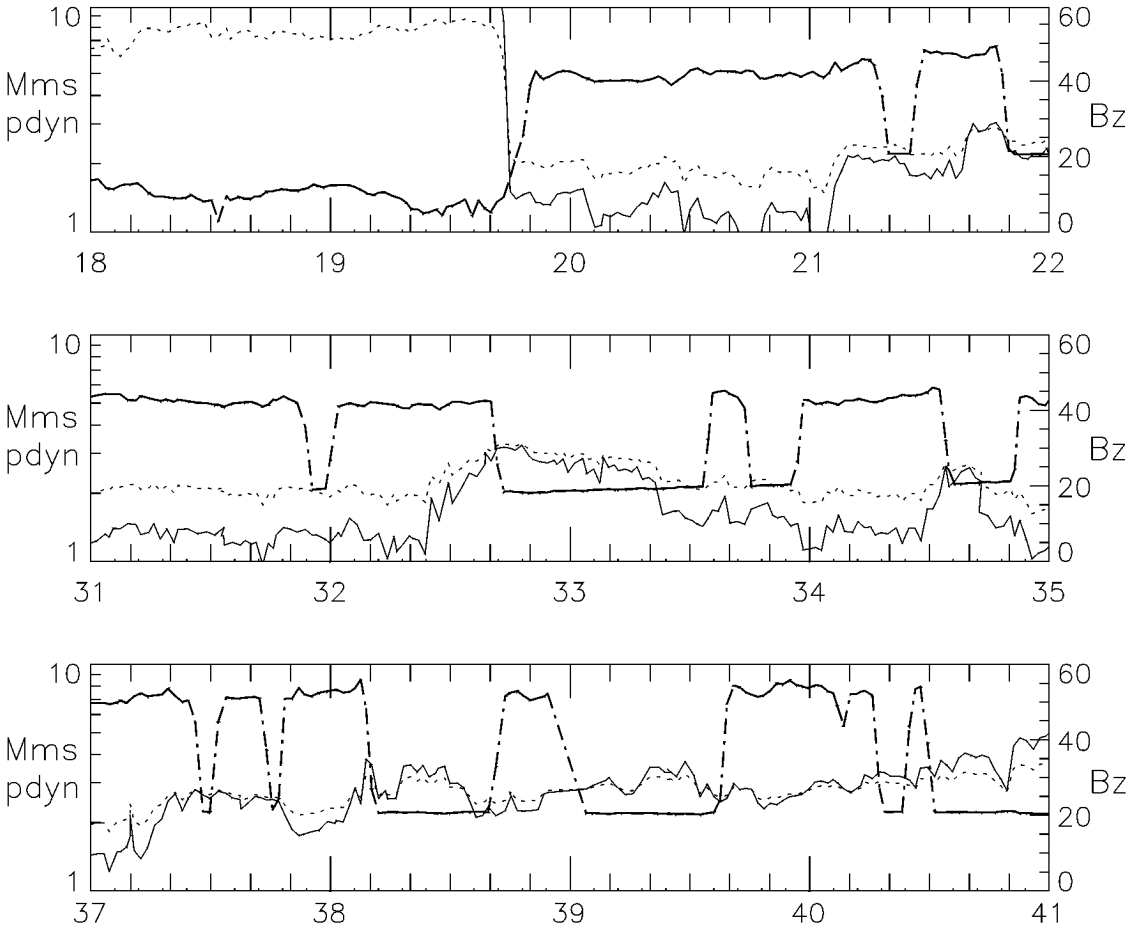

Figure 9. Dynamic pressure and magnetic field which show a delay between $p_{\rm dyn}$ and $M_{\rm ms}$ changes and bow shock reaction. The dotted dashed line marks the magnetic field, whereas the dotted line contributes to the magnetosonic Mach number and the solid line to the dynamic pressure.

plified solution also presented by *Grabbe and Cairns* [1995]

$$X = -\frac{C_a}{2}\left\{1 + \sqrt{1 - 4\left[\frac{(\gamma + \gamma\cos^2\theta - 2)}{(\gamma+1)\,C_a^2 M_{\rm A}^2}\right]}\right\} \quad (6)$$

with

$$C_{\rm A} = - \left\{\left(\frac{\gamma-1}{\gamma+1}\right) + \frac{2}{M_S^2}\left(\frac{1}{\gamma+1}\right) + \frac{\gamma + (\gamma+2)\cos^2\theta}{(\gamma+1)\,M_{\rm A}^2}\right\} \quad (7)$$

An empirical relation between the bow shock standoff distance (a_s), the magnetopause nose ($a_{\rm mp}$), and X takes the following form [*Cairns and Lyon,* 1995; *Farris and Russell,* 1994; *Seiff*, 1962; *Spreiter et al.,* 1966]

$$\frac{a_s}{a_{\rm mp}} = j + k\,X \quad (8)$$

For the gas dynamic empirical relation found by *Seiff* [1962] and further developed by *Spreiter et al.* [1966], $j = 1$ and $k = 1.1$, where the value of k depends on the obstacle shape. In the model presented by *Farris and Russell* [1994] the value for k is modified at lower Mach numbers by $k = 1.1\,M_{\rm ms}^2/(M_{\rm ms}^2 - 1)$, while j stays at 1. In the model developed from MHD simulations by *Cairns and Lyon* [1995], $j = 0.4$ and $k = 3.4$ for quasi-perpendicular flows with $M_S \sim 8$ and $M_{\rm A} > 1.5$. These values are appropriate for our problem, and so we calculate the ratio

$$\frac{a_s}{a_{\rm mp}} = 0.4 + 3.4\,X \quad (9)$$

using (6) and (7) for X.

Figure 10 shows $a_s/a_{\rm mp}$ during the passage of the cloud. The greatest value can be seen at about 2345 UT when Alfvén Mach number and dynamic pressure reach their lowest values. Compared with the predictions of *Cairns and Lyon* [1995, Figure 3] our results qualitatively agree fairly well in the studied range of $M_{\rm A}$ and $M_{\rm ms}$, respectively.

Figure 11 shows six panels where the first one contains the predicted a_s from (9) (solid line) and the given position dependent on $M_{\rm A}$, keeping the dynamic pressure at its average value for the first group of crossings. In the second panel we keep the Mach number at its average value for

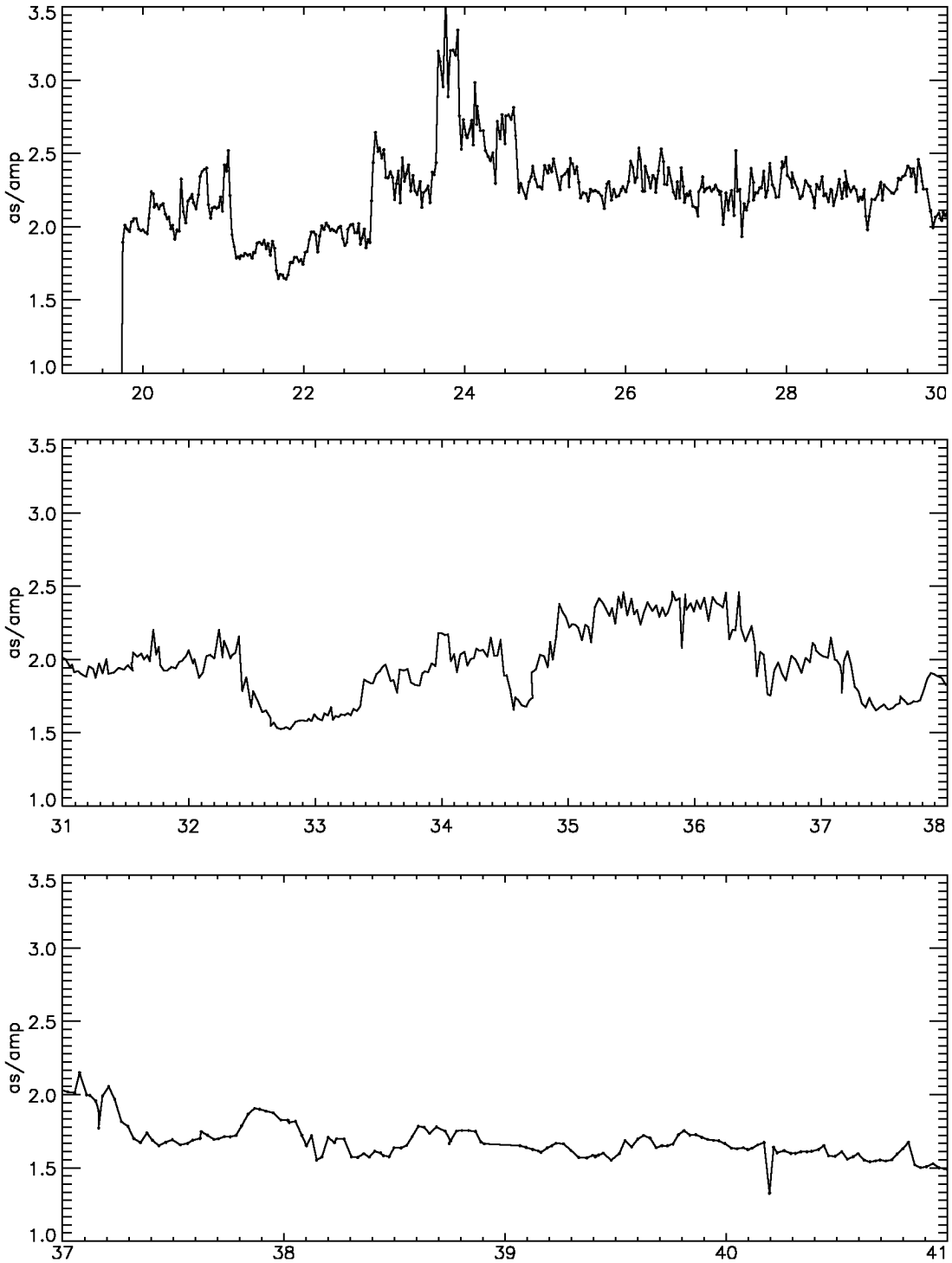

Figure 10. Values $a_s/a_{\rm mp}$ derived after *Grabbe and Cairns* [1995].

the group of crossings and check the effects of $p_{\rm dyn}$ through parameter $a_{\rm mp}$ in (9). The other four panels repeat this procedure for the other two groups of crossings. The most impressive thing which can be made out of this figure is that it seems that especially for the large upstream excursions of the bow shock, $M_{\rm A}$ influences the bow shock motion most. Of course, when looking at the solar wind parameters, this is an unexpected result, because of fairly constant values of B and the proportionality of $p_{\rm dyn}$ and $M_{\rm A}$ via the solar wind density and bulk speed ($M_{\rm A}^2 = \mu_0\,\rho\,v_{\rm sw}^2/B^2 = \mu_0\,p_{\rm dyn}/B^2$). Two considerations have to be taken into account when analyzing this figure: (1) a_s is calculated in subsolar distance,

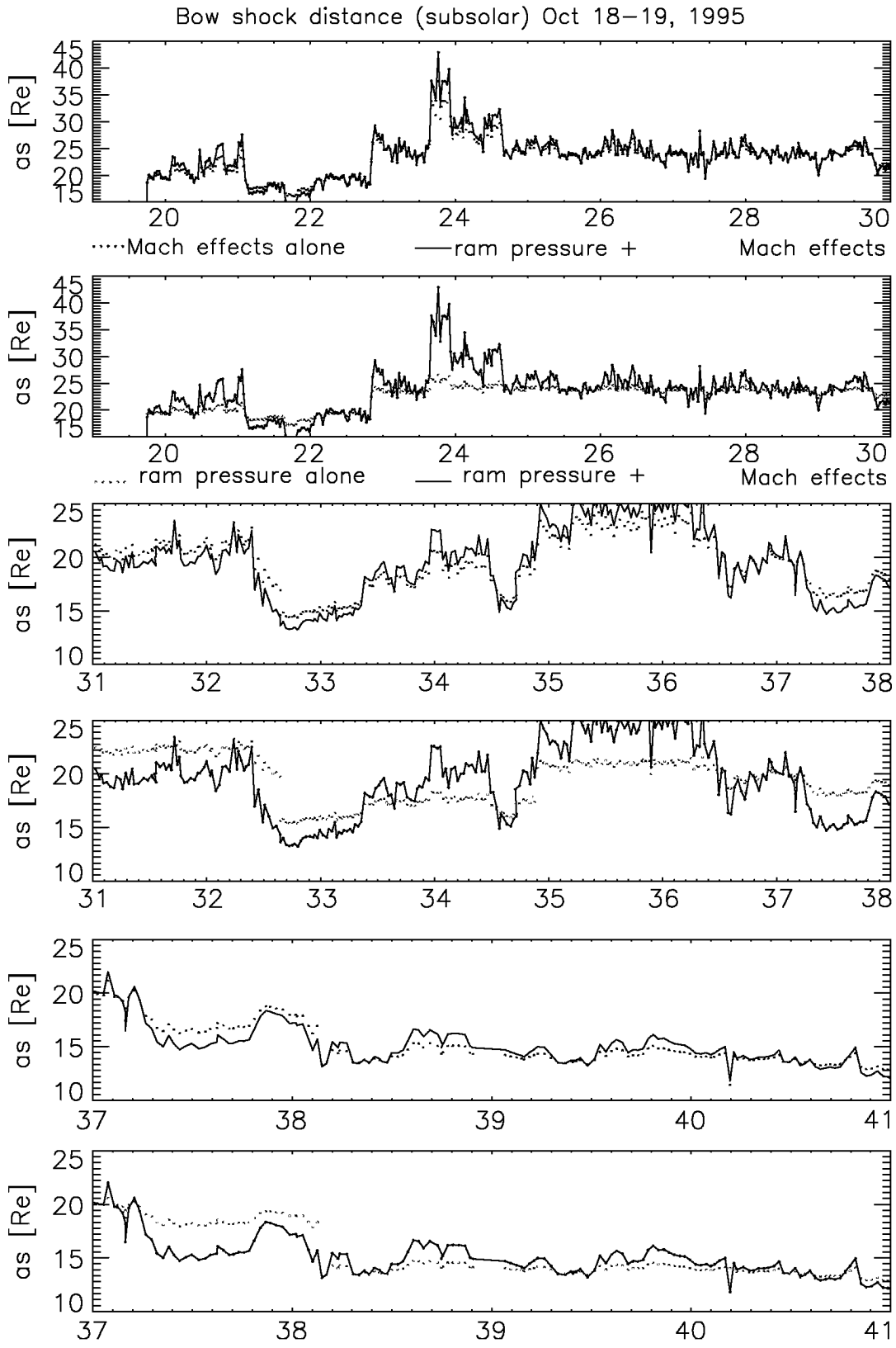

Figure 11. Bow shock standoff distance after *Grabbe and Cairns* [1995] (solid). Effects of M_A (every first panel, dotted) and p_{dyn} (every second panel, dotted).

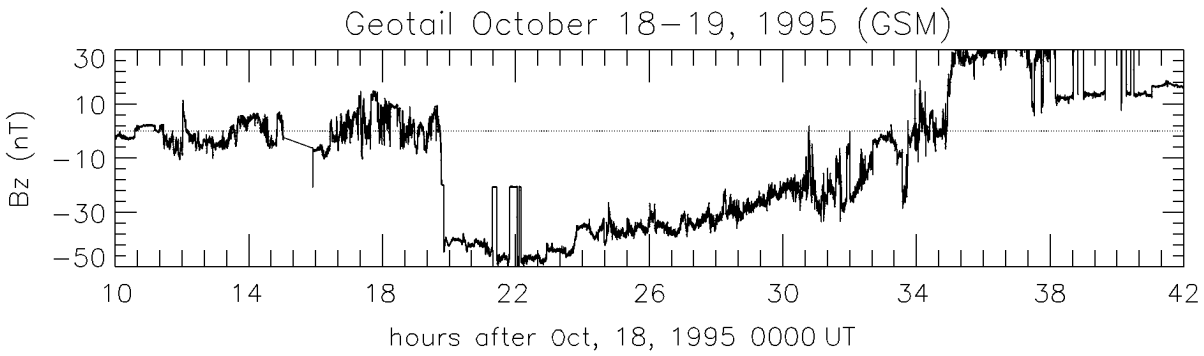

Figure 12. Geotail B_z component in GSM coordinates.

and our crossings are not subsolar; (2) to derive the nose of the magnetopause, we have used the formula for pressure balance, which might not give the most realistic behavior of the magnetopause for this event. The very large, negative B_z (see Figure 12) should lead to magnetic field line reconnection and to an erosion of the magnetosphere. Thus the magnetopause calculated from pressure balance should be an overestimation of the true standoff distance.

For Figure 13 we plotted four different ratios $a_s/a_{\rm mp}$ for the 26 measured bow shock crossings. The first one repeats the Cairns and Lyon formula (9), which takes into account the plasma and magnetic field data measured by Geotail. For the other three calculations the bow shock standoff distance is taken from the Geotail crossings brought to the subsolar line via the fitted bow shock shape described in (1). For the magnetopause standoff distance we use various calculations, which also underlay some restrictions, because of our set of solar wind data. In this way we combine actual measurements with theory and models, respectively. (1) *Shue et al.* [1998] (dotted line): This is a numerical formula that takes into account the possibility of erosion but is also restricted in the range of negative $B_z \geq -18$ nT; pressure balance (dashed line): This simple formula ignores B_z; (2) *Farrugia et al.* [1995] (dashed dotted line): The magnetopause is taken as a tangential discontinuity, which precludes reconnection. On the other hand, the relation was derived specifically for low Alfvén Mach number. The dependence of the magnetopause thickness is normalized to $a_{\rm mp}$ of $1/M_{\rm A}^2$, which is an important feature in our study.

From the figure we can see that for the first period, where we have very negative B_z, the Cairns and Lyon formula and the Shue et al. formula fit quite well; and in the third period with positive B_z, the Farrugia et al. magnetopause leads to rather good agreement with Grabbe and Cairns.

Conclusions

1. We examined 26 repeated crossings of the bow shock on 18–19 October 1995, made by Geotail.

2. The period studied corresponded to an Earth passage of an interplanetary magnetic cloud.

3. We related these crossings to interplanetary parameters, the solar wind dynamic pressure, and the solar wind Alfvén and magnetosonic Mach numbers. For the interval studied, the ranges of these parameters were $1 < M_{\rm ms} < 4$ and 0.2 nPa $< p_{\rm dyn} <$ 10 nPa, respectively. Thus we expect large sunward displacements of the bow shock.

4. Compared to the model bow shock of Farris et al., we find a net average sunward displacement of 1.85 R_E due to the low Alfvén Mach number.

5. We calculated the bow shock normals in two different ways and found that the coplanarity normals agree with the Farris et al. shape normals except near the flanks, where a wide scatter in the derived normals is observed.

6. All bow shock crossings were quasi-perpendicular, $\theta_{\rm av} \sim 75°$.

7. Small density jumps at bow shock occurred in association with low bow shock speed (of the order of 20 km s^{-1}).

8. We examine a delay in the response time of the bow shock between $M_{\rm ms}$ and $P_{\rm dyn}$ changes at Geotail and the bow shock crossings. This delay was of the order of ∼10–20 min.

9. Our results are in fair agreement with the simulations of Cairns and Lyon on the standoff bow shock position in relation to $M_{\rm ms}$.

10. We compare the position of the magnetopause and bow shock as predicted by various models and offered reasons for discrepancies between them.

11. The drawing of any conclusions due to the extreme conditions of the interplanetary magnetic field should also have been part of bow shock observations in this special magnetic cloud event. As seen from the data plots, there was strong negative B_z for a long period then rotating to the northward direction, also a strong eastward component rotating to strong westward values. However, reconnection might occur, the magnetopause could be eroded, and asymmetries in the Earth magnetosphere could play a nonnegligible role. This we point out in Figure 13, comparing the $a_s/a_{\rm mp}$ values in the first panel when B_z was less than zero. In this panel the result of the Cairns and Lyon model agrees rather well with the Shue et al. formula, which takes into account the direction of B_z. The pressure balance results show much lower values. Vice versa in the third panel with $B_z > 0$, the $a_s/a_{\rm mp}$ derived from the actual SW characteristics fit better with pressure balance than with Shue et al. Further work will be reported elsewhere [*Farrugia et al.,* 2001].

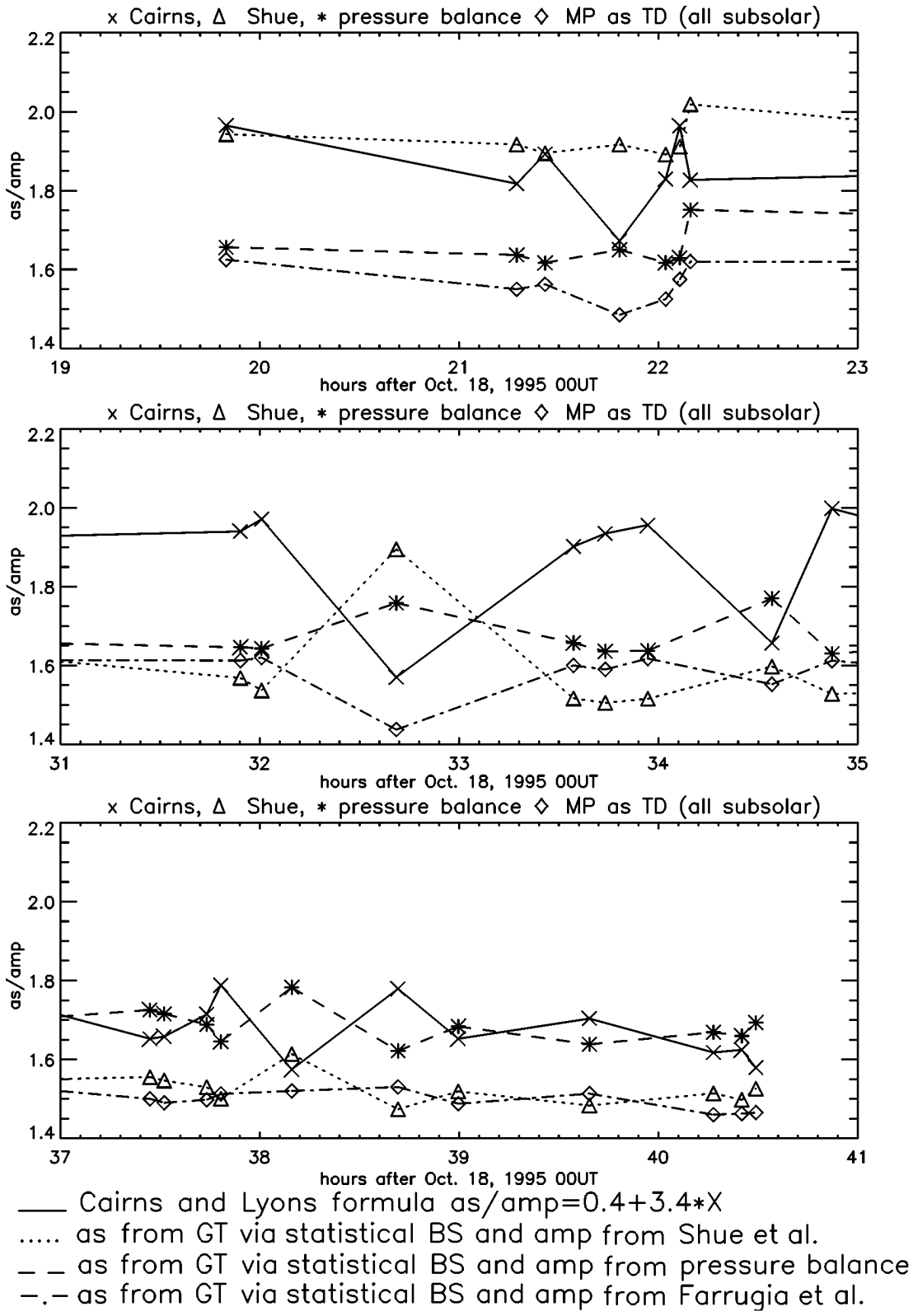

Figure 13. Values $a_s/a_{\rm mp}$ for the three periods of bow shock crossings derived in four different ways (see text above).

Acknowledgments. This work is partially supported by the INTAS-ESA project 99-01277, the Austrian "Fonds zur Förderung der wissenschaftlichen Forschung" under projects P13804-TPH and P12761-TPH, by NASA grant NAG5-2834, by grant 98-05-65290 from the Russian Foundation of Basic Research, by grant 97-0-13.0-71 from the Russian Ministry of Education, and by the Austrian Academy of Sciences, "Verwaltungstelle für Auslandsbeziehungen."

References

Abraham-Shrauner, B., and S. H. Yun, Interplanetary shock seen by Ames plasma probe on Pioneer 6 and Pioneer 7, *J. Geophys. Res., 81*, 2097, 1976.

Burgess, D., Collisionless Shocks, in *Introduction to Space Physics*, edited by M. G. Kivelson and C. T. Russell, Cambridge Univ. Press, New York, 1995.

Burlaga, L. F., Wind-Geotail magnetic cloud event: Summary October 18–20, 1995 (Days 291–293), http://bolero.gsfc.nasa.gov/~solart/cloud/summary.html, 1995.

Burlaga, L. F., E. Sittler, F. Mariani, and R. Schwenn, Magnetic loop behind an interplanetary shock: Voyager, Helios, and IMP 8 observations, *J. Geophys. Res., 86*, 6673, 1981.

Burlaga, L. F., et al., A magnetic cloud containing prominence material: January 1997, *J. Geophys. Res., 103*, 277, 1998.

Cairns, I. H., and C. L. Grabbe, Towards an MHD theory for the standoff distance of Earth's bow shock, *Geophys. Res. Lett., 21*, 2781, 1994.

Cairns, I. H., and J. G. Lyon, MHD simulations of Earth's bow shock at low Alfvén Mach numbers: Standoff distances, *J. Geophys. Res., 100*, 17,173, 1995.

Cairns, I. H., and J. G. Lyon, Magnetic field orientation effects on the standoff distance of Earth's bow shock, *Geophys. Res. Lett., 23*, 2883, 1996.

Cairns, I. H., D. H. Fairfield, R. R. Anderson, V. E. H. Carlton, K. I. Paularena, and A. J. Lazarus, Unusual locations of Earth's bow shock on September 24–25, 1987: Mach number effects, *J. Geophys. Res., 100*, 47, 1995.

Fairfield, D. H., Average and unusual locations of the Earth's magnetopause and bow shock, *J. Geophys. Res., 76*, 6700, 1971.

Farris, M. H., and C. T. Russell, Determining the Standoff Distance of the Bow Shock–Mach Number Dependence and Use of Models, *J. Geophys. Res., 99*, 17,681, 1994.

Farris, M. H., S. M. Petrinec, and C. T. Russell, The thickness of the magnetosheath: Constrains on the polytropic index, *Geophys. Res. Lett., 18*, 1821, 1991.

Farrugia, C. J., N. V. Erkaev, H. K. Biernat, and L. F. Burlaga, Anomalous magnetosheath properties during Earth passage of an interplanetary cloud, *J. Geophys. Res., 100*, 19,245, 1995.

Farrugia, C. J., et al., Geoeffectiveness of three Wind magnetic clouds: A comparative study, *J. Geophys. Res., 103*, 17,261, 1998.

Farrugia, C. J., et al., The bow shock on 18–19 October 1995, *J. Geophys. Res.*, in press, 2001.

Formisano, V., P. C. Hedgecock, G. Moreno, J. Sear, and D. Bollea, Observations of Earth's bow shock for low Mach numbers, *Planet. Space Sci., 19*, 1519, 1971.

Grabbe, C. L., Low Mach number predictions in an extended axially symmetric MHD theory of the magnetosheath, *Geophys. Res. Lett., 24*, 2495, 1997.

Grabbe, C. L., and I. H. Cairns, Analytic MHD theory for Earth's bow shock at low Mach numbers, *J. Geophys. Res., 100*, 19,941, 1995.

Kokubun, S., et al., Magnetic field measurement (MGF), in *Geotail Prelaunch Report, SES-TD-92-007SY*, pp. 58–70, Inst. of Space and Astronaut. Sci., SES Data Cent., Tokyo, Japan, 1992.

Lepping, R. P., J. A. Jones, and L. F. Burlaga, Magnetic field structure of interplanetary clouds at 1 AU, *J. Geophys. Res., 95*, 11,957, 1990.

Lepping, R. P., et al., The Wind magnetic field investigation, *Space Sci. Rev., 71*, 207, 1995.

Lepping, R. P., et al., The Wind magnetic cloud and events of October 18–20, 1995: Interplanetary properties and as triggers for geomagnetic activity, *J. Geophys. Res., 102*, 14,049, 1997.

Mukai, T., S. Machida, N. Kaya, T. Terasawa, T. Obara, A. Nishida, M. Ejiri, M. Hirahara, and Y. Saito, Low energy particle experiment (LEP), in *Geotail Prelaunch Report, SES-TD-92-007SY*, pp. 97–125, Inst. of Space and Astronaut. Sci., SES Data Center, Tokyo, Japan, 1992.

Ogilvie, K. W., et al., SWE, a comprehensive plasma instrument for the Wind spacecraft, *Space Sci. Rev., 71*, 55, 1995.

Peredo, M., J. A. Slavin, E. Mazur, and S. A. Curtis, Three-dimensional position and shape of the bow shock and their variation with Alfvénic, sonic and magnetosonic Mach number and interplanetary magnetic field orientation, *J. Geophys. Res., 100*, 7907, 1995.

Russell, C. T., and S. M. Petrinec, Comments on "Towards an MHD theory for the standoff distance of Earth's bow shock" by I. H. Cairns and C. L. Grabbe, *Geophys. Res. Lett., 23*, 309, 1996a.

Russell, C. T., and S. M. Petrinec, Comments on "Unusual locations of Earth's bow shock on September 24–25, 1987: Mach number effects" by I. H. Cairns, D. H. Fairfield, R. R. Anderson, V. E. H. Carlton, K. I. Paularena, and A. J. Lazarus, *J. Geophys. Res., 101*, 7677, 1996b.

Seiff, A., Gas dynamics in space exploration, in *NASA Space Publ., 24*, 1962.

Shue, J.-H., et al., Magnetopause location under extreme solar wind conditions, *J. Geophys. Res., 103*, 17,691, 1998.

Spreiter, J. R., A. L. Summers, and A. Y. Alksne, Hydromagnetic flow around the magnetosphere, *Planet. Space Sci., 14*, 223, 1966.

P. Aber, Faculty of Arts and Sciences, Harvard University, Cambridge, MA 02138, USA.

H. K. Biernat, S. Mühlbachler, and D. F. Vogl, Space Research Institute, Austrian Academy of Sciences, Schmiedlstraße 6, Graz 8042, Austria; Institute for Geophysics, Astrophysics, and Meteorology, University of Graz, Universitätsplatz 5, 8010 Graz, Austria. (helfried.biernat@oeaw.ac.at)

N. V. Erkaev, Institute of Computational Modelling, Russian Academy of Sciences, Krasnojarsk 660036, Russia. (erkaev@ksc.krasn.ru)

C. J. Farrugia and J. M. Quinn, Institute of the Study of Earth, Oceans, and Space, University of New Hampshire, Durham, NH 03824, USA.

S. Kokubun, Solar-Terrestrial Environment Laboratory, Nagoya University, Nagoya, Japan.

R. P. Lepping and K. W. Ogilvie, NASA Goddard Space Flight Center, Greenbelt, MD 20771, USA.

T. Mukai, Institute of Space and Astronautical Science, Kanagawa, Japan.

V. S. Semenov, Physics Research Institute, St. Petersburg State University, St. Petersburg 198904, Russia. (sem@snoopy.phys.spbu.ru)

(Received 3 May 2001; accepted 4 July 2001)